*J Mater Sci: Mater Electron* (2024) 35:867

# Synthesis, analysis and characterizations of $Dy^{3+}$ ions-doped $CaBi_2Nb_2O_9$ phosphors for optoelectronic device applications

Sheetal Kumari[1], Pooja Rohilla[1], Samarthya Diwakar[2], Rupesh A. Talewar[3], Ankur Shandilya[4], Yasha Tayal[5], K. Swapna[6], Aman Prasad[2,*], and A. S. Rao[1]

[1] *Department of Applied Physics, Delhi Technological University, Bawana Road, Delhi 110042, India*
[2] *Department of Physics and Computer Science, Dayalbagh Educational Institute (DEI), Deemed University, Dayalbagh, Agra 282005, India*
[3] *Department of Physics, Shri Ramdeobaba College of Engineering and Management, Katol Road, Nagpur 440013, India*
[4] *Department of Physics, Hindu College, University of Delhi, Delhi 110007, India*
[5] *ABES Engineering College, Ghaziabad 201009, India*
[6] *Department of Physics, Koneru Lakshmaiah Education Foundation, Vaddeswaran, Guntur 522502, India*

**Received:** 9 November 2023
**Accepted:** 21 April 2024



## ABSTRACT

The current study focuses on the synthesis and other detailed studies on $CaBi_2Nb_2O_9$ (abbreviated CBNO) phosphor doped with $Dy^{3+}$ ions. The aforementioned phosphors were prepared via a solid-state reaction procedure and a comprehensive analysis of the crystal structure, particle morphology, vibrational bands, luminous characteristics, decay and thermal stability of the phosphors was done. Phase identification of the synthesized material was carried out using X-ray diffraction (XRD) technique and the optical bandgap was determined using diffuse reflectance spectra (DRS). The morphological studies and particle size estimation of the phosphor material were conducted using a scanning electron microscope (SEM). Under 452 nm excitation, the photoluminescence (PL) spectra of $Dy^{3+}$-doped CBNO phosphor exhibit three peaks at 482, 576, and 666 nm, which correspond to the transitions $^4F_{9/2} \rightarrow {}^6H_{15/2}$, $^6H_{13/2}$, and $^6H_{11/2}$. The electric dipole–dipole interaction was the main mechanism for concentration quenching for $Dy^{3+}$ ions. The estimated CIE chromaticity coordinates for $Dy^{3+}$ ion-doped CBNO phosphors fall in the white region. The temperature-dependent PL (TD-PL) findings reveals that CBNO phosphors have a considerably superior thermal stability. The results of these investigations suggest that the CBNO phosphors doped with $Dy^{3+}$ ions exhibit promising properties that could be used for prospective w-LEDs and other optoelectronic device applications.

Address correspondence to E-mail: amanprasad2891@gmail.com

https://doi.org/10.1007/s10854-024-12640-2
Published online: 28 April 2024

## 1 Introduction

The development of a variety of inorganic phosphors appropriate for white light-emitting diodes (w-LEDs) has progressively drawn a great deal of interest to promote the area of solid-state lighting and other display related applications by virtue of their excellent luminescence, low operating voltage, and chemical and thermal durability. [1–7]. It is well known that the w-LEDs are regarded as the fourth generation of SSL and are a better alternative to conventional incandescent, and fluorescent lamps. w-LEDs have received plenty of attention and have been the subject of extensive research because of their unique benefits, which include environmental protection, short response times, high luminous efficiencies, long lifespans, reliability, and lack of mercury. Usually $Y_3Al_5O_{12}$: $Ce^{3+}$ (YAG: Ce) phosphors, which emit yellow light, are combined with blue light from n-UV LED chips to produce commercially available w-LEDs [1, 6, 8–11]. The lack of red colour in this setup results in a low colour rendering index (CRI) and a high colour temperature (CCT). This is inefficient for general room lighting as well. Researchers are concentrating on pc-w-LEDs through tricolour (blue, green, and red) phosphors coated on n-UV chips to get greater CRI and lower CCT in order to solve this drawback [12–14]. For significant red nitride phosphors used in w-LEDs ($SrLiAl_3N_4$: $Eu^{2+}$, $CaAlSiN_3$: $Eu^{2+}$, and $Ca_2Si_5N_8$: $Eu^{2+}$), the synthesis requires a demanding environment, such as high pressure and high temperature. Commercial red phosphor ($Y_2O_2S$: $Eu^{3+}$) used in it, however, has several intrinsic drawbacks due to colour re-absorption and distinct degradation such as low luminous efficiency and unstable CCT respectively [15–19]. The mild synthesis environment and generally stable chemical properties of the oxide materials make them useful for a variety of applications. A single-phase white-light-emitting phosphor stimulated effectively with n-UV LED chip is widely preferred to solve the challenges mentioned above, and in the last few decades, this desire has attracted the attention of numerous research groups.

Dysprosium oxide ($Dy_2O_3$), one of the known rare earth ions, is crucial for emission in white region since it may be easily activated by UV or blue LED chips. $Dy^{3+}$ exhibits blue ($^4F_{9/2} \rightarrow {}^6H_{15/2}$), yellow ($^4F_{9/2} \rightarrow {}^6H_{13/2}$) and red ($^4F_{9/2} \rightarrow {}^6H_{11/2}$) emission bands at wavelengths of 482 nm, 575 nm, and 666 nm, respectively [9, 20–24]. Also, $^4F_{9/2} \rightarrow {}^6H_{13/2}$ has a higher intensity but, it is less sensitive to the environment of the ligand. $^4F_{9/2} \rightarrow {}^6H_{15/2}$ is hypersensitive but, it is greatly impacted by the environment of the host, and $^4F_{9/2} \rightarrow {}^6H_{11/2}$ is least affected by the environment of the host. Many phosphor materials are being studied for their yellow to blue (Y/B) intensity ratio since it must be equal to one to satisfy the need for pure white light emission. Various $Dy^{3+}$ ions-doped phosphors, including $SrAl_2O_4$ [16], $KBaY(BO_3)_2$ [15], and $SrLaAlO_4$ [17], that possess a high absorption in the n-UV range and emit white light, have already been reported.

Nowadays, a wide variety of host materials, including phosphates, silicates, borates, vanadates, fluorides, ceramics, niobates, and tungstates can be doped with RE ions. Due to its great chemical stability, good thermal stability, and eco-friendliness, niobate is regarded as a dependable host material. In general, niobium oxides have a low phonon frequency [25, 26]. The likelihood of the non-radiative transition can be efficiently lowered, that lends the phosphors their strong fluorescence [27]. The Aurivillius-type bismuth layered structure ferroelectrics (BLSFs), whose chemical formula is $(Bi_2O_2)^{2+}$ $(A_{m-1}B_mO_{3m+1})^{2-}$, have drawn a lot of interest because of their comparatively high Curie point ($T_c$), which translates to high thermal stability [28, 29]. CBNO is a member of the BLSF family with $m = 2$, where $Ca^{2+}$ is present at site A and $Nb^{5+}$ is present at site B of the pseudo-perovskite $(CaNb_2O_7)^{2-}$ blocks. CBNO has a stacking $(Bi_2O_2)^{2+}$ layer and perovskite $(CaNb_2O_7)^{2-}$ units with double $NbO_6$ octahedral layers [30]. It was proposed that the perovskite blocks could accommodate a wide range of cations, but the bismuth oxide layers were difficult to alter [28]. However, no research has been done on the CBNO: $Dy^{3+}$ phosphor for fabricating white LEDs.

The main aim of this research work is to generate white light with improved luminosity. In this work, the high temperature solid-state method was used to synthesis a series of $Dy^{3+}$ ions-doped CBNO phosphors. The structural and spectroscopic characteristics of phosphors were investigated using a variety of characterisation techniques, including XRD, UV–Vis, PL emission, decay profiles and TD-PL. FT-IR studies were employed to understand various vibrational groups present in the CBNO phosphor. From the PL emission data, the CIE chromaticity coordinates were carefully examined. As far as we are aware, there hasn't been any information published about the luminescence characteristics of $Dy^{3+}$-doped CBNO phosphors. The aforementioned characteristics suggest that

white light-emitting CBNO phosphor may be utilised in the fabrication of w-LEDs and other optoelectronic device applications.

## 2 Material preparation and instrumentation

The CBNO: x $Dy^{3+}$ ($x = 0.01, 0.02, 0.03, 0.04,$ & $0.05$ mol) ions-doped phosphors were prepared by solid-state reaction process. Starting raw materials $CaCO_3$ (Thermo fisher 98%), $Bi_2CO_3$ (Loba Chemie 99%), $Nb_2O_5$ (Loba Chemie 99.9%), $Dy_2O_3$ (Central Drug House 99.9%), are used. These materials were weighed with their stoichiometric ratio and ground for an hour in an agate mortar. Acetone is employed as a wetting medium. The ground powder was put in an alumina crucible, heated in a high temperature programmable muffle furnace at 1250 °C for 5.5 h, and then allowed to cool at ambient temperature. After that process, the final collected powder was reground again for 10 min to obtain the homogeneous mixture for further characterization purposes.

The chemical reaction of synthesis process can be described by the following chemical formula:

$$CaCO_3 + Nb_2O_5 + Bi_2CO_3 = CaBi_2Nb_2O_9 + \text{gases}$$

The XRD patterns of the as-titled samples were recorded using the Bruker Model D8 Advance instrument with Nickel filtered Cu-K$\alpha$ radiation (1.54 Å). Using the JEOL 7610 F Plus machine, SEM records for surface morphology were taken. A Perkin-Elmer Frontier FT-IR spectrometer was employed for analysing the FT-IR spectra. A JASCO model V-923 UV–Vis-NIR spectrophotometer (± 2.0 nm resolution) was utilized to record the DRS for the as-titled phosphors. A Jasco FP-8300 spectrofluorometer with a Xenon excitation source having 1.0 nm resolution was used to study the PL excitation and emission spectra. The PL decay profiles were analysed using an Edinburgh FL920 fluorescence spectrometer. The Flame-S-XR1-ES spectrometer from Ocean Optics was utilised to study TD-PL spectra. All measurements except TD-PL were made at the room temperature. The flowchart of the steps involved in the preparation of the phosphor by the solid-state reaction method is shown in Fig. 1.

## 3 Results and discussion

### 3.1 XRD analysis

The initial assessment of the purity of the as-prepared sample was conducted using XRD. Figure 2a illustrates the XRD patterns of the undoped CBNO host material. All the diffraction peaks in the sample can be attributed to the standard data for CBNO (ICDD no. 49-0608). No signs of any other phases were detected, indicating that the obtained samples consist of a single phase. $CaBi_2Nb_2O_9$ exhibits an

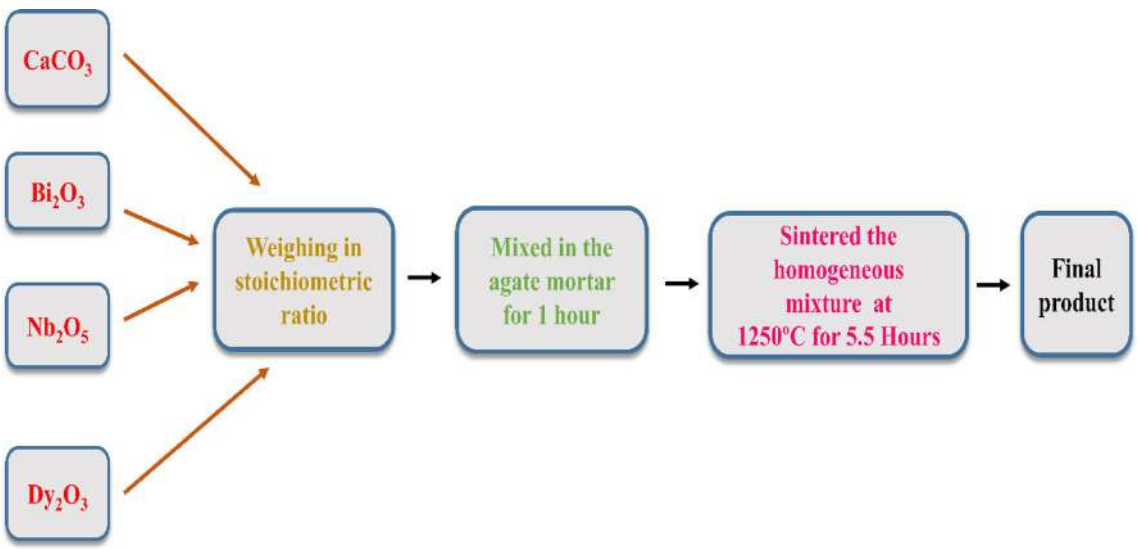


**Fig. 1** Flow chart of the steps involved in the synthesis of CBNO phosphor

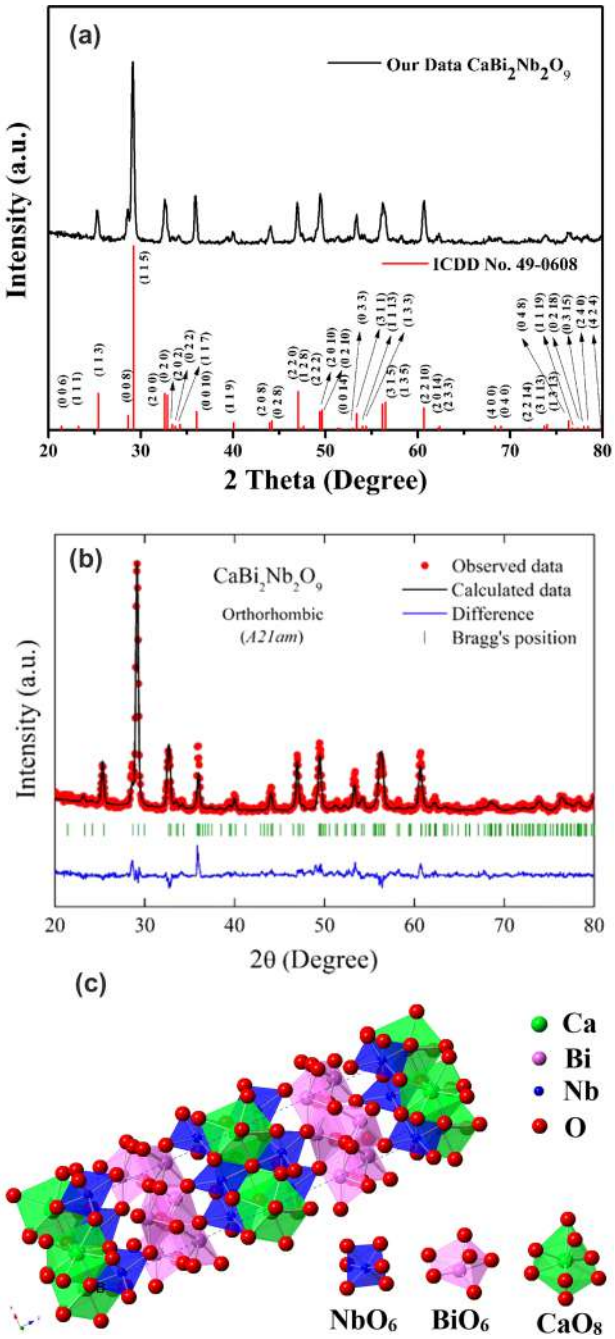


**Fig. 2** **a** XRD pattern of the $CaBi_2Nb_2O_9$ and the reference data of ICDD no. 49–0608 **b** Reitveld refinement pattern of an un-doped CBNO phosphor **c** Crystal structure of $CaBi_2Nb_2O_9$, emphasizing the coordination environment of Ca, Bi and Nb atoms

orthorhombic crystal structure with a space group of $A2_1am$, featuring lattice parameters $a = 5.4827$ Å, $b = 5.4415$ Å, $c = 24.8974$ Å, and $\alpha = \beta = \gamma = 90°$.

**Table 1** Calculated structural lattice and rietveld refinement parameters of CBNO phosphor

| Parameters | Standard data JCPDS | CBNO (un-doped) | Reference |
|---|---|---|---|
| Formula | $CaBi_2Nb_2O_9$ | $CaBi_2Nb_2O_9$ | [18, 34] |
| Crystal system | $A2_1am$ (36)—Orthorhombic | $A2_1am$ (36)—Orthorhombic | |
| Crystal density (gm $cm^{-1}$) | 7.499 | 7.499 | |
| Units, Z | 4 | 4 | |
| a (Å) | 5.4827 | 5.4406(3) | |
| b (Å) | 5.4415 | 5.4722(3) | |
| c (Å) | 24.8974 | 24.8527(8) | |
| $\alpha = \beta = \gamma$ | 90° | 90° | |
| Cell volume, V ($Å^3$) | 742.79 | 739.9161(3) | |
| GOF | | 2.54 | |

To further assess the phase purity of the synthesized samples, Rietveld refinement was employed, using CBNO as a representative. Rietveld refinement is a method that involves analyzing profile measurements of powder intensity to approximate the phosphor's structural model. The initial model was constructed based on previously reported crystallographic data for CBNO [31]. Figure 2b depicts Rietveld refinement plots for $CaBi_2Nb_2O_9$ powders, which were prepared using the solid-state reaction method and heat-treated at 1250 °C for 5.5 h. The observed XRD patterns closely match the theoretical fit results, indicating the success of the Rietveld refinement method. The refined crystallographic parameters align well with the reflection conditions, and the fit is highly satisfactory with $\chi^2 = 2.54$, confirming the phase purity of the as-prepared sample and $\chi 2$ value is less than the other reported papers [32, 33]. The smaller value of $\chi^2$ indicates that a single phase has been formed. Table 1 provides the structural parameters of the Rietveld refinement, including crystal structure, space group, lattice parameters and goodness of fit ($\chi^2$) [18, 34]. The term $\chi^2$ serves as a measure of the goodness of fit (GOF), indicating how well the experimental XRD patterns align with the calculated ones. Table 2 presents the atomic coordinates and the occupancy of cations and anions in the CBNO compound [31]. Following the refinement process, crystal structures of the CBNO compound were generated using the output.cif file with the Vesta software, as depicted in Fig. 2c.

**Table 2** Atomic coordinates, cation and anion occupancies of a CBNO compound

| Atom | x | y | z | Site occupancy factor (SOF) | References |
|---|---|---|---|---|---|
| Ca | − 0.0763 | 0.2526 | 0.0000 | 0.5 | [31] |
| Bi | 0.4543 | 0.7742 | 0.2000 | 1 | |
| Nb | 0.4910 | 0.7434 | 0.4152 | 1 | |
| O1 | 0.5056 | 0.3009 | 0.0000 | 0.5 | |
| O2 | 0.5854 | 0.6483 | 0.3311 | 1 | |
| O3 | 0.7535 | 0.9968 | 0.2528 | 1 | |
| O4 | 0.7345 | 0.9832 | 0.9303 | 1 | |
| O5 | 0.7857 | 0.9676 | 0.5880 | 1 | |

Figure 2c illustrates the crystal structure of CBNO, highlighting the arrangement of $Ca^{2+}$, $Bi^{3+}$, and $Nb^{5+}$ atoms in their respective coordination environments. CBNO belongs to the Aurivillius-type materials, characterized by a pseudo-perovskite structure. This category was initially identified by Aurivillius in 1949. As explained in the introduction, the crystal structure of CBNO has $Ca^{2+}$ ions occupying the A site and $Nb^{5+}$ ions occupying the B site. The crystal structure of CBNO is composed of chains of $CaO_8$ octahedra that share edges and run parallel to the a-axis. According to structural data, calcium ions have a coordination number of 8, while bismuth and niobium ions have a coordination number of 6. The ionic radii for 8-coordinated $Ca^{2+}$ and 6-coordinated $Bi^{3+}$ are 1.12 Å and 1.03 Å, respectively. Consequently, due to their similar ionic radii and valence, it is anticipated that $Dy^{3+}$ ion dopants, with a 6-coordinated structure and an ionic radius of 0.912 Å, will substitute for $Bi^{3+}$ ions within the host structure.

## 3.2 Morphological studies

The microscopic shape and particle size of the as-prepared phosphors have also been further examined using SEM. Figure 3a, b shows the SEM pictures of the

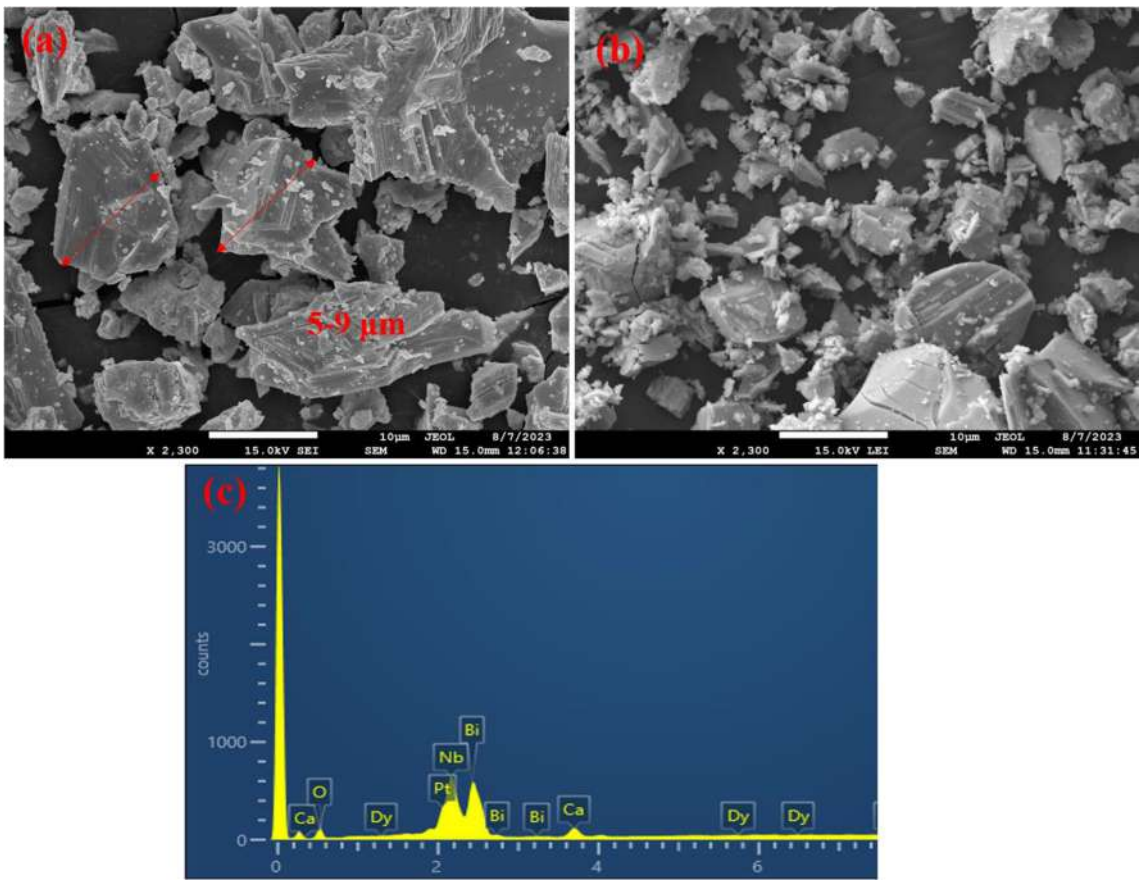


**Fig. 3** **a**–**b** SEM images recorded for 0.04 mol of $Dy^{3+}$ ions-doped CBNO phosphor, **c** corresponding EDS image

CBNO: 0.04 mol $Dy^{3+}$-doped phosphor. The irregular shape of the phosphor is evident in Fig. 3. Due of the high-temperature reaction and grinding procedure, the synthesised materials show agglomeration. Today's commercially available phosphor particles are typically between two 2–10 μm (μm) in size. The as-prepared phosphor samples have an average particle size in the 5–9 μm range as has been highlighted in the image. Also, the phosphor particles with size ranges in μm have been considered more convenient for use in pc w-LEDs. Energy dispersive spectrum (EDS) used to monitor the elemental composition of the as-titled phosphor is depicted in Fig. 3c. The EDS image shows that every precursor element is present in the material. The different colours, i.e. green, purple, yellow, and blue corresponding to Dy, Bi, Nb, and Ca, respectively are depicted in Fig. 4. These results demonstrate the equally distribution of the components in the as-prepared phosphors.

## 3.3 FT-IR analysis

Figure 5 shows the FT-IR spectrum for the CBNO: 0.04 mol $Dy^{3+}$-doped phosphor. FT-IR spectrum was captured to reveal information about the functional groups found in the CBNO phosphor. It contains peaks at 545, 610, 797, 1071 and 2974 $cm^{-1}$. The band centred at 610 $cm^{-1}$ can be assigned to Nb–O of the $NbO_6$ octahedral stretching vibration [34]. The octahedral $NbO_6$ peak indicates single-phase formation.

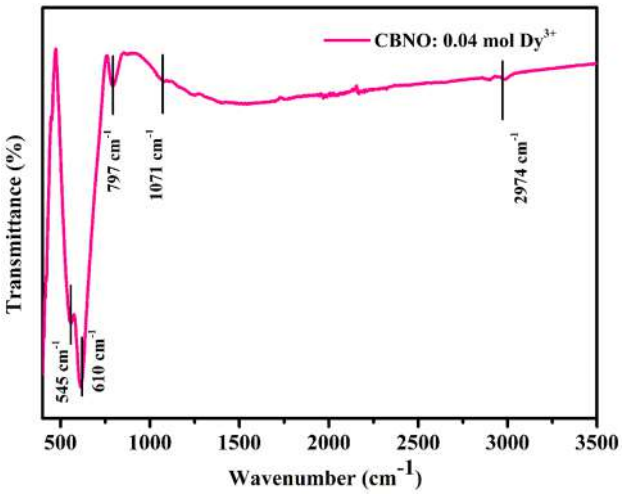


**Fig. 5** FT-IR spectrum of CBNO: 0.04 mol $Dy^{3+}$ ion-doped phosphor

The stretching vibration mode of Bi-$O_3$ is attributed to the shoulder peak at 545 $cm^{-1}$ [35]. The stretching vibration mode of Nb–$O_5$ and the bending vibration mode of $O_4$–Nb–$O_5$ correspond to the shoulder peaks at 797 and 1071 $cm^{-1}$, respectively [18, 35]. The hydrogen bonding is attributed to the band was seen in the region 2700–3000 $cm^{-1}$.

## 3.4 DRS analysis

Phosphors used in w-LEDs depend significantly on the optical bandgap (Eg). Figure 6 displays the DRS

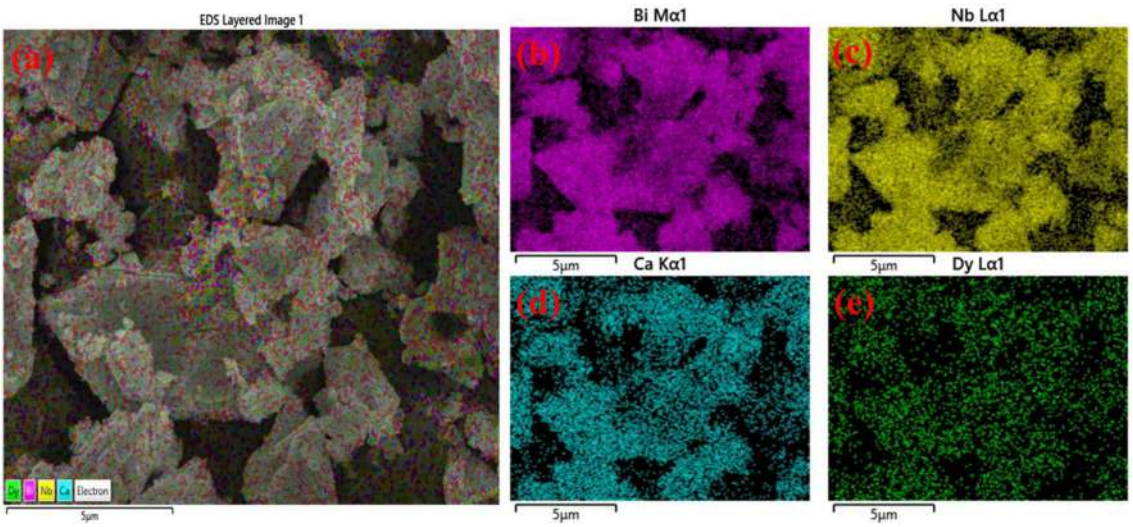


**Fig. 4** **a** The total element distribution map, **b–e** shows the relative element points of various colours against a dark background; purple, yellow, blue and green, correspond to Bi, Nb, Ca, and Dy, respectively (Color figure online)

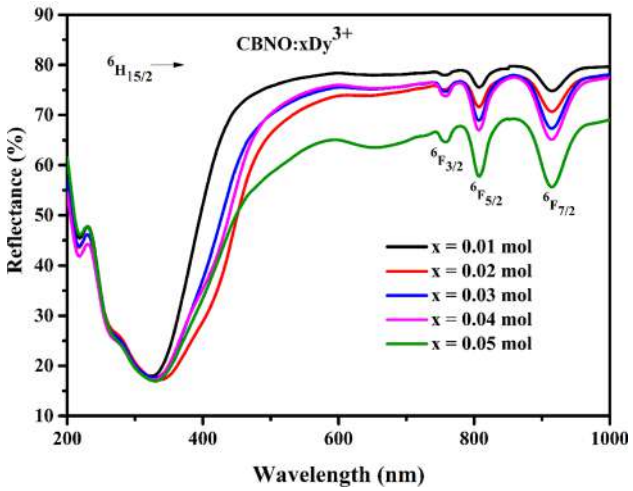


**Fig. 6** DRS of CBNO: xDy$^{3+}$ ($x$ = 0.01, 0.02, 0.03, 0.04, & 0.05 mol) phosphors

for CBNO: x Dy$^{3+}$ ($x$ = 0.01, 0.02, 0.03, 0.04, & 0.05 mol) phosphors samples in the range 200–1000 nm. The charge transfer (CT) from the oxygen (2p) to the empty 4f orbital of the Dy$^{3+}$ ion in the host can be seen by two absorption lines observed at wavelengths of 219 nm and 264 nm. The peaks observed in the spectra at 756 nm, 808 nm & 915 nm correspond to the transitions from $^6H_{15/2}$ to $^6F_{3/2}$, $^6F_{5/2}$, & $^6F_{7/2}$ respectively. Carnall et al. have validated each of the aforementioned band designations. [36].

Bandgap determination actually helps us to understand parameters like stability, lifetimes and degradation of the material. This knowledge is essential for deploying materials in various photonic, SSL and solar cell applications. Using the equation below, the $E_g$ was estimated by transforming the DRS data into the Kubelka–Munk function [37].

$$F(R) = \frac{(1-R^2)}{2R} = \frac{\alpha}{S} \quad (1)$$

Here $\alpha$ stands for the absorption coefficient, $R$ for the samples' reflectance, and $S$ for the scattering coefficient. The Tauc equation, which determines the energy bandgap ($E_g$) and absorption coefficient ($\alpha$), is shown below [8].

$$\alpha h\nu = C\left(h\nu - E_g\right)^n$$

Here $C$ stands for the energy-independent constant (= 1), and hν represents the photon energy. $n$ can have value of 2 for indirect or 1/2 for direct transition.

Since F(R) and $\alpha$ are directly related, the equation above can be rewritten as follows [8]:

$$F(R)h\nu = C\left(h\nu - E_g\right)^n \quad (2)$$

The optical bandgap for the Dy$^{3+}$ ions-doped CBNO phosphors using a Tauc plot which was drawn between the $[F(R)\ h\nu]^2$ and hν. The $E_g$ can be estimated by extrapolating the linear region of the plot. The direct bandgap values evaluated for CBNO: x Dy$^{3+}$ ($x$ = 0.01, 0.02, 0.03, 0.04, & 0.05 mol) phosphors are 4.59, 4.57, 4.56, 4.54, and 4.51 eV, respectively and shown in Fig. 7. Thus, it can be concluded that CBNO phosphor is viable host lattice because of its high bandgap and may find utility in w-LEDs applications. The $E_g$ value slightly decreases with an increase in Dy$^{3+}$ ion concentration, which may be due to the 4f energy level of Dy$^{3+}$ ions [38].

### 3.5 PL studies

It is vital to know the proper excitation wavelength in order to analyse the PL spectra of Dy$^{3+}$-doped CBNO phosphor. Excitation spectrum of the as-prepared CBNO: 0.04 mol Dy$^{3+}$-doped phosphor measured at an emission wavelength of 576 nm in the 300–500 nm range is shown in Fig. 8. In that, PL excitation peaks were observed from the ground state $^6H_{15/2}$ to various excited states $^4M_{17/2}$, $^6P_{7/2}$, $^6P_{5/2}$, $^4F_{7/2}$, $^4G_{11/2}$, $^4I_{15/2}$ and $^4F_{9/2}$ at 311, 354, 367, 389, 428, 452 and 478 nm respectively [32, 39–41]. The strongest excitation peak was seen at a wavelength of 452 nm. Therefore, emission spectra for all of the Dy$^{3+}$-doped CBNO phosphors were analysed at this wavelength.

PL emission spectra for CBNO: x Dy$^{3+}$ ($x$ = 0.01, 0.02, 0.03, 0.04, & 0.05 mol) phosphors were recorded at 452 nm excitation in the range 470–700 nm as shown in Fig. 9. In the PL spectra, three emission peaks were seen at wavelengths of 482 nm, 576 nm, and 666 nm, corresponding to the $^4F_{9/2} \rightarrow {}^6H_{15/2}$, $^6H_{13/2}$, and $^6H_{11/2}$ transitions, respectively [9, 42]. The position of the peaks do not significantly alter with increasing Dy$^{3+}$ ion concentration because the 5 s and 5p outer electrons shield the 4f electrons. Among three distinctive peaks, it can be seen that the emission at 576 nm dominates and is the source of yellow colour emission. As Dy$^{3+}$ concentration rises up to 0.04 mol, the emission intensity also rises. Beyond 0.04 mol of Dy$^{3+}$ ions, concentration quenching due to non-radiative energy transfer between

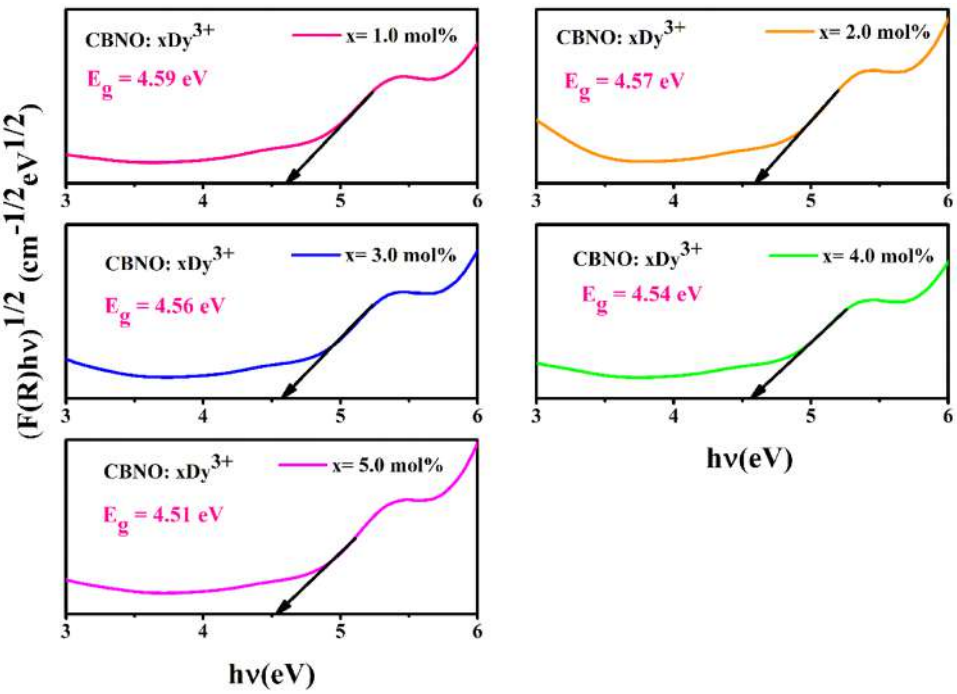


**Fig. 7** Tauc plot for direct optical bandgap of CBNO phosphors at different concentrations of $Dy^{3+}$ ions

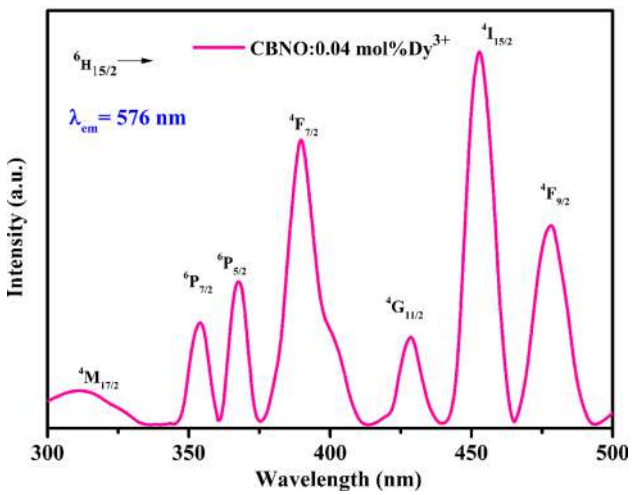


**Fig. 8** Excitation spectrum of CBNO: 0.04 mol Dy3 +-doped phosphor under 576 nm emission wavelength

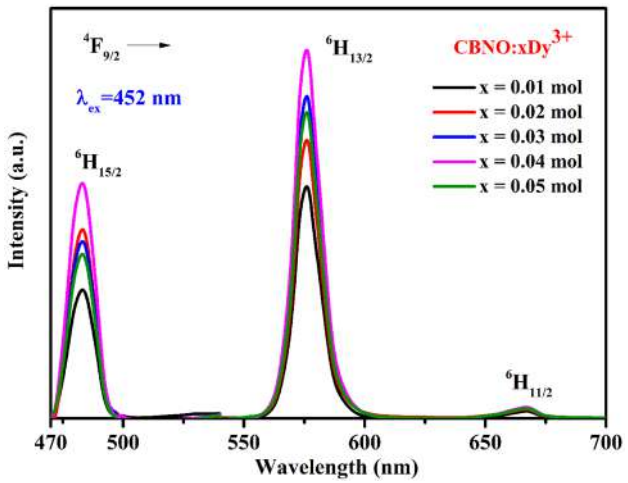


**Fig. 9** PL emission spectra of CBNO: $xDy^{3+}$ ($x$=0.01, 0.02, 0.03, 0.04, & 0.05 mol) at $\lambda_{ex}$=452 nm

$Dy^{3+}$–$Dy^{3+}$ ions led to a drop in PL intensity. Radiation re-absorption, exchange contact, and multipole-multipole interaction between the activator ions are the reasons that cause concentration quenching.

The critical distance ($R_c$) is assessed to comprehend the kind of interaction that occurs between $Dy^{3+}$ ions. Using Blasse's equation, the Rc is computed [43].

$$R_c \approx 2\left[\frac{3V}{4\pi x_c N}\right]^{1/3} \quad (3)$$

Here V stands for the unit cell volume, N is the number of cations per unit cell and $x_c$ is the optimum concentration of the RE ions. After putting all the values, i.e. $V$ = 748.68 Å$^3$, $x_c$ = 0.04 mol, & $N$ = 4, $R_c$ was found to be 20.71 Å. A multipolar electric contact

between the $Dy^{3+}$ ions arises during the energy transfer if the value of $R_c$ is more than 5Å [44].

The type of multipolar interaction has been estimated from Dexter hypothesis, which suggests a relationship between variation in emission intensity and concentration of RE ions [45].

$$\log\left(\frac{I}{x}\right) = \log f - \frac{Q\log(x)}{3} \quad (4)$$

Here, Q stands for the type of interaction that takes place between the dopant ( 6, 8, or 10 denoting electric dipole–dipole (D–D), dipole-quadrupole (D–Q), and quadrupole–quadrupole (Q–Q), respectively) and A is a constant, too. The (Q/3) value is calculated using the slope of the linear fitting curve log(I/x) vs log(x), as demonstrated in Fig. 10. The computed Q value is 4.82 which is very near to 6, suggests that electric D–D interaction is the reason for concentration quenching and consequent energy transfer between $Dy^{3+}$ ions.

Figure 11 displays the energy level diagram of the CBNO phosphor, which also covers the mechanisms for emission, excitation, energy transfer, and cross relaxation channels (CRC). The $Dy^{3+}$ ions are first excited to higher excited levels as part of the emission mechanism, which is followed by a rapid relaxation to the metastable state $^4F_{9/2}$ level via non-radiative transfers. From the $^4F_{9/2}$ excited state, radiative transfers take place to various low energy states, such as $^6H_{15/2}$, $^6H_{13/2}$, and $^6H_{11/2}$. CRC and resonance energy transfer (RET) in the CBNO phosphor may result in concentration quenching and non-radiative energy transfer.

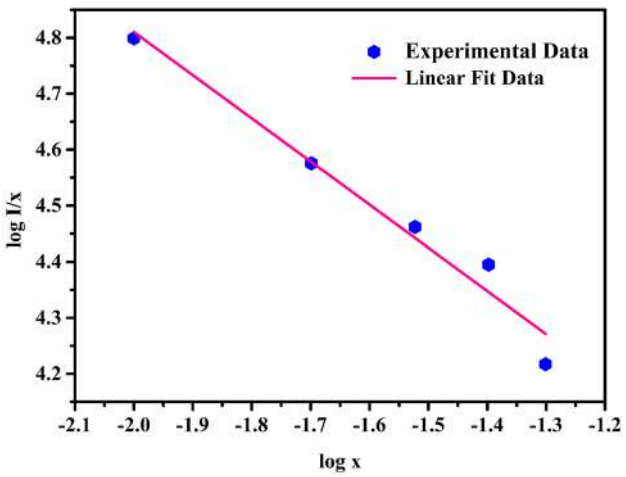


**Fig. 10** Plot of log (I/x) with log(x)

## 3.6 CIE chromaticity coordinates

The colour of a phosphor is determined using Commission Internationale de l'Eclairclage (CIE) coordinates. The variations in the concentration of $Dy^{3+}$ have no impact on the position of the emission peaks, but influence the intensity of the PL emission. Figure 12 displays the CIE coordinates of every $Dy^{3+}$ ion-doped CBNO phosphor sample at $\lambda_{ex} = 452$ nm and $\lambda_{em} = 576$ nm, which are in the white area at ambient temperature. They have also been tabulated in Table 3 [17, 46, 47]. From the CIE chromaticity analysis, it can be concluded that these as prepared phosphors are acceptable for the manufacture of white LEDs.

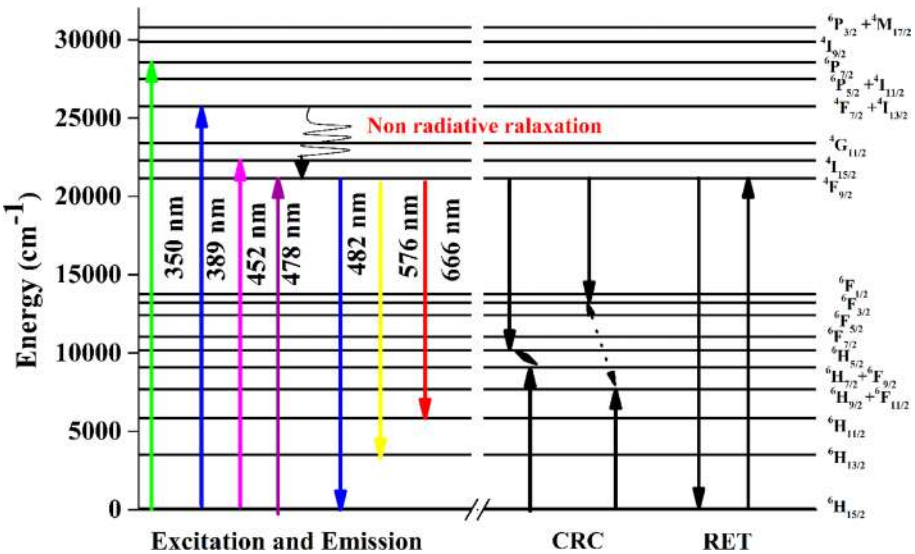


**Fig. 11** Partial energy level diagram and possible cross-relaxation channels of $Dy^{3+}$-doped CBNO phosphor

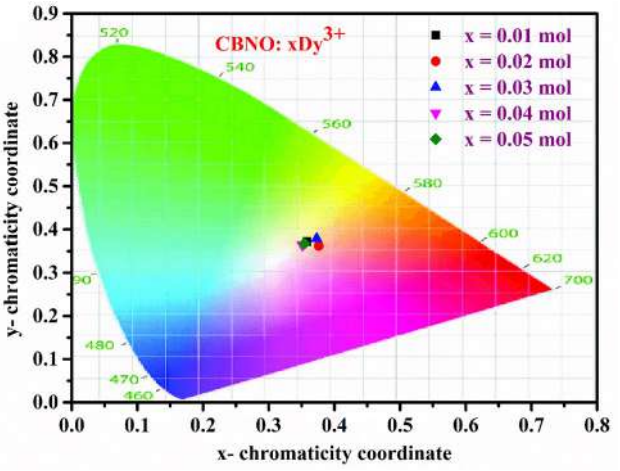


**Fig. 12** CIE chromaticity coordinates for CBNO: $xDy^{3+}$ ($x$ = 0.01, 0.02, 0.03, 0.04, & 0.05 mol) phosphors under $\lambda ex$ = 452 nm

Correlated colour temperature (CCT) is another significant indicator for emphasising the usage and significance of $RE^{3+}$-doped phosphor. CCT is the colour temperature of white light emitted by the phosphor. A low or high CCT indicates that the light being emitted is either warm or cold, respectively.

McCamy provided a formula for calculating CCT given below [9]:

$$CCT = -449n^3 + 3525n^2 - 6823.2n + 5520.3 \quad (5)$$

Here, $n = \frac{x-xe}{y-ye}$ and ($x_e$, $y_e$) refers to the colour coordinate of white illumination ($x_e$ = 0.332, $y_e$ = 0.186) and (x, y) stands for colour coordinates of the as-titled phosphor. Table 3 shows the CCT values of $Dy^{3+}$-doped CBNO phosphor at $\lambda_{ex}$ = 452 nm. The calculated CCT values of the CBNO:$xDy^{3+}$ phosphors is significantly less than 5000 K, indicating that warm white light can be created from these phosphors.

Colour purity (CP) is a significant factor in colourimetric calculations. The saturation and level of vibrant colour are described by CP. Following equation is used to evaluate the CP [48]:

$$CP = \frac{\sqrt{(x - x_{ee})^2 + (y - y_{ee})^2}}{\sqrt{(x_d - x_{ee})^2 + (y_d - y_{ee})^2}} \quad (6)$$

where ($x_{ee}$, $y_{ee}$) stand for equal energy point, (x, y) are colour coordinates of the optimized phosphor, and ($x_d$, $y_d$) denotes points of dominant wavelength. The calculated CP values for all the phosphors lie between 14 to 22%. These values are small and have been tabulated in Table 3. Owing to the low values of CP, it can be used in photonic devices as an n-UV pumped white emitting component [49].

## 3.7 Decay profiles

PL decay curves for CBNO: x $Dy^{3+}$ ($x$ = 0.01, 0.02, 0.03, 0.04, & 0.05 mol) phosphors under $\lambda_{ex}$ = 452 nm and $\lambda_{em}$ = 576 nm are shown in Fig. 13. The best fit to the measured decay curves is tri-exponential equation which is given below [50]:

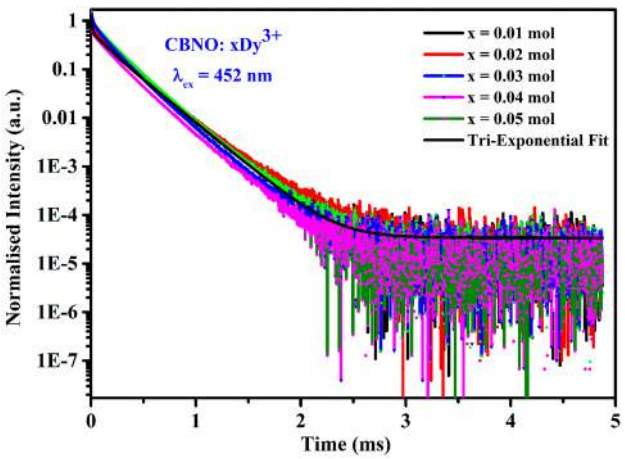


**Fig. 13** PL decay profiles for CBNO: $xDy^{3+}$ ($x$ = 0.01, 0.02, 0.03, 0.04, & 0.05 mol) phosphors under $\lambda ex$ = 452 nm

**Table 3** CIE coordinates, CCT values & colour purity of CBNO: $xDy^{3+}$ ($x$ = 0.01, 0.02, 0.03, 0.04, & 0.05 mol) under 452 nm excitation wavelength

| Sample ID CBNO: $xDy^{3+}$ | CIE coordinates ( x, y) | CCT values (K) | Colour purity (%) | $\tau_{avg}$ (μs) | References |
|---|---|---|---|---|---|
| $x$ = 0.01 mol | (0.3579,0.3719) | 4275.087 | 18.2 | 220.85 | [17, 46, 47, 51] |
| $x$ = 0.02 mol | (0.3761,0.3622) | 4218.556 | 21.1 | 215.81 | |
| $x$ = 0.03 mol | ( 0.3729,0.3789) | 3992.671 | 17.6 | 198.79 | |
| $x$ = 0.04 mol | (0.3508,0.3639) | 4163.508 | 14.3 | 194.41 | |
| $x$ = 0.05 mol | (0.3543,0.3675) | 3898.664 | 16.7 | 185.63 | |

$$I = I_0 + A_1 * \exp\left(-\frac{t}{\tau_1}\right) + A_2 * \exp\left(-\frac{t}{\tau_2}\right) + A_3 * \exp\left(-\frac{t}{\tau_3}\right) \quad (7)$$

where $I_0$ and I are the PL intensity at time $t = 0$ and time t, respectively. $\tau_1$, $\tau_2$ and $\tau_3$ denote the decay lifetimes and $A_1$, $A_2$ & $A_3$ denote the constants for fitting. The average decay time ($\tau_{avg}$) has been calculated with the formula given below [50, 51]

$$\tau_{avg} = \frac{A_1\tau_1^2 + A_2\tau_2^2 + A_3\tau_3^2}{A_1\tau_1 + A_2\tau_2 + A_3\tau_3} \quad (8)$$

The evaluated values of $\tau_{avg}$ have been presented in Table 3.The values of $\tau_{avg}$ decrease with the increase in doping ions demonstrating the possibility of energy transfer between $Dy^{3+}$ ions [52]. As the doping concentration rises, the spacing between $Dy^{3+}$ ions gets smaller. The luminescence lifetime decreases due to an increase in the nonradiative interaction between activator ions.

### 3.8 TD-PL studies

The TD-PL spectra of CBNO: 0.04 mol $Dy^{3+}$-doped phosphor were recorded under 452 nm excitation wavelength between 25 and 175ºC to study the thermal quenching behaviour and have been displayed in Fig. 14 along with the varying temperature. The PL emission intensity was seen to be decreasing with increasing temperature. At 175 ºC, the phosphor retained 48.2% of its maximal light intensity, demonstrating remarkable thermal stability.

To further assess the thermal characteristics of the sample, the activation energy (ΔE) was also measured. The value of ΔE was calculated by using the Arrhenius equation [53]

$$I_T = \frac{I_0}{1 + C\exp\left(-\frac{\Delta E}{K_B T}\right)} \quad (9)$$

Here, $I_0$ and $I_T$ represent the intensity at temperature 25 ºC and the intensity at a specific temperature T and $K_B$ denotes Boltzmann constant. The value of the activation energy (ΔE) is obtained from the slope of the of graph shown for $\ln((I_0/I_T)-1)$ versus $1/K_BT$, as depicted in Fig. 15. The calculated activation energy for CBNO: 0.04 mol $Dy^{3+}$-doped phosphor was 0.287 eV which is greater than other values in literature [12, 54, 55]. The high value of activation energy indicates that the as-prepared phosphor is more stable thermally. As a result, TD-PL spectra for the CBNO: 0.04 mol $Dy^{3+}$-doped phosphor demonstrated the excellent temperature stability [42].

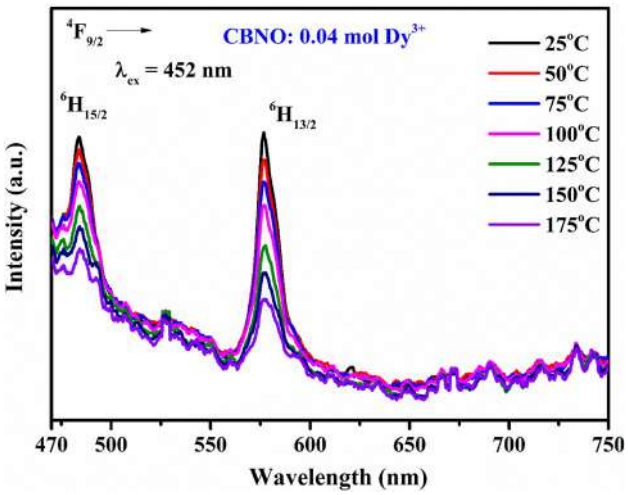


**Fig. 14** TD-PL spectra for 0.04 mol $Dy^{3+}$-doped CBNO phosphor at 452 nm excitation wavelength from RT to 175 ºC

## 4 Conclusion

In conclusion, $Dy^{3+}$-doped CBNO phosphors were effectively synthesised using the solid-state reaction technique. The XRD analysis verifies the single phase formation of $Dy^{3+}$-doped CBNO phosphors. Morphological study was carried out using SEM, and the particle size was determined to be in the micrometre range. EDS indicates that all the elements were evenly distributed over the crystal's surface. FT-IR spectrum for $Dy^{3+}$-doped phosphor demonstrate the presence of vibrational bands. The optical bandgap of the as-titled phosphors was seen to decrease with an increase in the quantity of $Dy^{3+}$ ions, owing to their 4f energy level. The $Dy^{3+}$-doped CBNO phosphors show emission peaks at wavelengths of 482, 576, and 661 nm when excited at a wavelength of 452 nm, which are attributable to distinct transitions of the $Dy^{3+}$ ions. For CBNO phosphor, the optimal $Dy^{3+}$ concentration was found to be 0.04 mol beyond which quenching takes place. The calculated CIE coordinates for all of the $Dy^{3+}$ ion-doped CBNO phosphor samples at $\lambda_{ex} = 452$ nm and $\lambda_{em} = 576$ nm lie in the white region. A tri-exponential behaviour is observed in the decay curves of the as-prepared phosphors under stimulation at 452 nm.

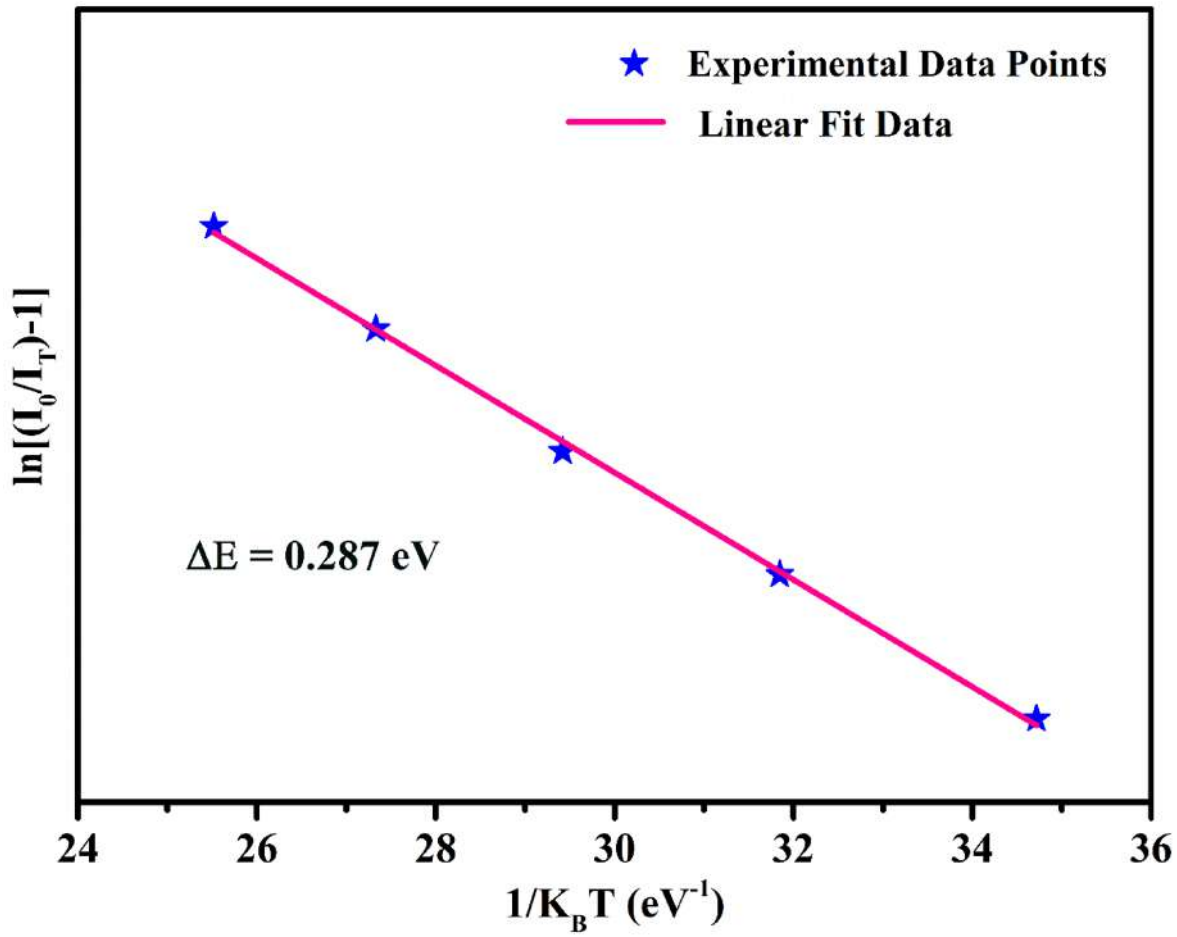


**Fig. 15** Linear relationship of ln $[(I_0/I_T)-1]$ versus $1/K_BT$

The thermal stability of the phosphors was evaluated by TD-PL measurements. It was observed that a high activation energy was needed for thermal quenching in the phosphors. The experimental findings show that the CBNO phosphor doped with $Dy^{3+}$ ions has at potential for usage in the fabrication of w-LEDs and other optoelectronic devices.

## Acknowledgements

The author is very thankful to CSIR-UGC for giving her a Junior Research Fellowship (UGC Ref. 1431/CSIR-UGC NET JUNE 2019). Dr. Aman Prasad is grateful to Dayalbagh Educational Institute (DEI), Deemed University, Agra for providing a Research Seed Money Grant (DEI/GBMF(3052022)/518). We are also grateful to Dr. Shayama Prasad and Dr. Manju Srivastava in the Department of Chemistry at Dayalbagh Educational Institute (DEI), Deemed University, Agra for making the FESEM facility available to us.

## Author contributions

Sheetal Kumari: Experimentation, data analysis, manuscript writing. Pooja Rohilla: Experimentation, data analysis. Samarthya Diwakar: Synthesis, experimentation. Rupesh Talewar: Data Analysis,
Ankur Shandilya: Data Analysis. Yasha Tayal: Experimentation, data analysis. K. Swapna: Data analysis. Aman Prasad: Work plan, supervision, review, data analysis. A.S. Rao: Data analysis, review.

## Data availability

The data that support the findings of this study are available on request from the corresponding author Dr. Aman Prasad. The data are not publicly available due to restrictions, e.g. their containing information that could compromise the privacy of research participants.

## Declarations

**Competing interests** The authors declare that they have no known competing financial interests or personal relationships that could have appeared to influence the work reported in this paper.

## References


1. J. Wu, M. Li, H. Jia, M. Wang, Z. Liu, J. Lumin. **214**, 116607 (2019)
2. N. Deopa, M.K. Sahu, P.R. Rani, R. Punia, A.S. Rao, J. Lumin. **222**, 117166 (2020)
3. G. Wu, J. Xue, X. Li, Q. Bi, M. Sheng, Z. Leng, Ceram. Int. **49**, 10615 (2023)
4. J. Guo, J. Guo, J. Gao, J. Chen, Y. Yang, Y. Yang, L. Zheng, Y. Li, L. Zhao, B. Deng, R. Yu, Ceram. Int. **48**, 26992 (2022)
5. V.R. Prasad, S. Damodaraiah, S. Babu, Y.C. Ratnakaram, J. Lumin. **187**, 360 (2017)
6. S. Sarathkumar, S. Munimasthani, U.S.U. Thampy, R.V.S.S.N. Ravikumar, J. Mater. Sci. Mater. Electron. **31**, 11589 (2020)
7. X. Huang, J. Liang, S. Rtimi, B. Devakumar, Z. Zhang, Chem. Eng. J. **405**, 126950 (2021)
8. P. Rohilla, A.S. Rao, Mater. Res. Bull. **150**, 111753 (2022)
9. L. Zhou, L. Liu, R. Yang, J. Kong, Y. Li, Y. Zhao, Y. Du, C. Li, Z. Zou, B. Deng, R. Yu, Inorg. Chem. Commun. **148**, 110316 (2023)
10. R. Yu, Y. Guo, L. Wang, H.M. Noh, B.K. Moon, B.C. Choi, J.H. Jeong, J. Lumin. **155**, 317 (2014)
11. S. Dai, D. Zhao, R. Zhang, L. Jia, Q. Yao, J. Alloys Compd. **891**, 161973 (2021)
12. L. Wu, Y. Bai, L. Wu, H. Yi, Y. Kong, Y. Zhang, J. Xu, RSC Adv. **7**, 1146 (2017)
13. P. Rohilla, A.S. Rao, J. Mater. Sci. Mater. Electron. **34**, 1 (2023)
14. S. Adachi, J. Lumin. **202**, 263 (2018)
15. B. Han, Y. Dai, J. Zhang, B. Liu, H. Shi, Ceram. Int. **44**, 14803 (2018)
16. K.G. Kumar, P.B. Bhargav, K. Aravinth, R. Arumugam, P. Ramasamy, J. Lumin. **223**, 117126 (2020)
17. P. Sehrawat, A. Khatkar, P. Boora, M. Kumar, R.K. Malik, S.P. Khatkar, V.B. Taxak, Ceram. Int. **46**, 16274 (2020)
18. S.R. Alharbi, M. Alhassan, O. Jalled, S. Wageh, A. Saeed, J. Mater. Sci. **53**, 11584 (2018)
19. T. Sakthivel, G. Annadurai, R. Vijayakumar, X. Huang, J. Lumin. **205**, 129 (2019)
20. H. George, N. Deopa, S. Kaur, A. Prasad, M. Sreenivasulu, M. Jayasimhadri, A.S. Rao, J. Lumin. **215**, 116693 (2019)
21. M. Monisha, N. Mazumder, G. Lakshminarayana, S. Mandal, S.D. Kamath, Ceram. Int. **47**, 598 (2021)
22. W.J. Huang, J.H. Lei, Y.H. Chen, J.Y. Chen, Y. Li, L.P. Chen, H. Guo, Ceram. Int. **49**, 9799 (2023)
23. S. Damodaraiah, R.P. VL, Y.C. Ratnakaram, Optik (Stuttg) **192**, 162980 (2019)
24. A. Ichoja, S. Hashim, S.K. Ghoshal, Optik (Stuttg) **218**, 165001 (2020)
25. Z. Shen, C. Qin, W. Luo, F. Song, Z. Wang, Y. Li, S. Zhang, J. Mater. **6**, 459 (2020)
26. T.S. Sreena, P.P. Rao, A.K.V. Raj, T.R.A. Thara, J. Alloys Compd. **751**, 148 (2018)
27. H. Zou, Y. Hu, X. Zhu, D. Peng, X. Chai, J. Mater. Sci. Mater. Electron. **28**, 11921 (2017)
28. C. Qin, Z. Yang, S. Wen, Q. Luo, F. Sheng, S. Yan, H. Zhu, M. Wang, Y. Ming, J. Mater. Sci. Mater. Electron. **29**, 7801 (2018)
29. M. Ferroelectrics, D. Peng, H. Zou, C. Xu, J. Li, X. Wang, X. Yao, J. Appl. Phys. (2013). https://doi.org/10.1063/1.4818793
30. R. Tang, J. Kong, L. Zheng, Z. Wang, J. Guo, X. Jin, X. Hu, N. Gong, B. Deng, R. Yu, Mater. Res. Bull. **154**, 111925 (2022)
31. K. Miura, Appl. Phys. Lett. **80**, 2967 (2002)
32. P. Kumar, S. Singh, I. Gupta, K. Nehra, V. Kumar, D. Singh, Mater. Chem. Phys. **295**, 127035 (2023)
33. J. Song, T. Yang, H. Zhang, Y. Xiang, R. Song, B. Wang, J. Zhu, J. Lumin. **257**, 119664 (2023)
34. H.C. Gupta, V. Luthra, Vib. Spectrosc. **56**, 235 (2011)
35. O. Jalled, Z. Alharbi, S.R. Alharbi, A. Saeed, M. Alhassan, S. Al-Heniti, H.Y. Mohammed, Y. Al-Hadeethi, F. Al-Marzouki, A. Al-Mujtaba, J. Nanosci. Nanotechnol. **17**, 594 (2017)
36. W.T. Carnall, P.R. Fields, K. Rajnak, J. Chem. Phys. **49**, 4424 (1968)
37. S. Kumari, A.S. Rao, R.K. Sinha, Mater. Res. Bull. **167**, 112419 (2023)
38. N. Deopa, A.S. Rao, J. Lumin. **194**, 56 (2018)

39. E.A. Rathnakumari, S.M.M. Kennedy, J. Lumin. **235**, 118018 (2021)
40. S. Kaur, A.S. Rao, M. Jayasimhadri, Mater. Res. Bull. **116**, 79 (2019)
41. S. Kaur, D. Arora, S. Kumar, G. Singh, S. Mohan, P. Kaur, P.K. Kriti, D.P. Singh, J. Lumin. **202**, 168 (2018)
42. S. Kumari, A. Anu, P.R. Prasad, A.S. Rao, J. Mater. Sci. Mater. Electron. **34**, 907 (2023)
43. X. Meng, S. Huang, M. Shang, Inorg. Chem. Commun. **113**, 107768 (2020)
44. J. Zhao, S.X. Huang, D. Zhao, C.H. Huang, M.J. Ma, R.J. Zhang, Y.C. Fan, B.Z. Liu, J.W. Gao, Q. Zong, Y.P. Yu, Optik (Stuttg) **159**, 115 (2018)
45. S. Kaur, N. Deopa, A. Prasad, R. Bajaj, A.S. Rao, Opt. Mater. (Amst) **84**, 318 (2018)
46. X. Qin, X. Liu, W. Huang, M. Bettinelli, X. Liu, Chem. Rev. **117**, 4488–527 (2017)
47. E.A. Rathnakumari, S.M.M. Kennedy, Optik (Stuttg) **275**, 170601 (2023)
48. S. Kumari, A.S. Rao, R.K. Sinha, J. Mol. Struct. **1295**, 136507 (2024)
49. K. Poria, R. Lohan, S. Bhatia, A. Kumar, R. Singh, N. Deopa, R. Punia, J.S. Shahi, A.S. Rao, RSC Adv. **13**, 11557 (2023)
50. G. Jyothi, K.G. Gopchandran, Ceram. Int. **43**(15), 12044–12056 (2017)
51. X. Li, C. Liang, S. Guo, Y. Xiao, C. Chang, J. Lumin. **188**, 199 (2017)
52. X. Zhang, R. Cui, J. Zhang, G. Yuan, X. Qi, C. Deng, Optik (Stuttg). **245**, 167646 (2021)
53. K. Maheshwari, A.S. Rao, Opt. Mater. (Amst) **137**, 113533 (2023)
54. G. Zhu, Z. Li, F. Zhou, C. Wang, S. Xin, J. Lumin. **196**, 32 (2018)
55. B. Ma, X. Ma, T. Xu, K. Su, Q. Zhang, RSC Adv. **8**, 14164 (2018)